Editors' Suggestion   Featured in Physics

Observation of Photoion Backward Emission in Photoionization of He and N₂

Sven Grundmann [ORCID],[1,*] Max Kircher,[1,†] Isabel Vela-Perez,[1] Giammarco Nalin [ORCID],[1] Daniel Trabert [ORCID],[1] Nils Anders,[1] Niklas Melzer [ORCID],[1] Jonas Rist,[1] Andreas Pier,[1] Nico Strenger,[1] Juliane Siebert,[1] Philipp V. Demekhin [ORCID],[2] Lothar Ph. H. Schmidt,[1] Florian Trinter,[3,4] Markus S. Schöffler,[1] Till Jahnke,[1] and Reinhard Dörner [ORCID][1,‡]

[1]*Institut für Kernphysik, Goethe-Universität, Max-von-Laue-Strasse 1, 60438 Frankfurt, Germany*
[2]*Institute of Physics and Center for Interdisciplinary Nanostructure Science and Technology (CINSaT), University of Kassel, Heinrich-Plett-Strasse 40, 34132 Kassel, Germany*
[3]*Photon Science, Deutsches Elektronen-Synchrotron (DESY), Notkestrasse 85, 22607 Hamburg, Germany*
[4]*Molecular Physics, Fritz-Haber-Institut der Max-Planck-Gesellschaft, Faradayweg 4-6, 14195 Berlin, Germany*

We experimentally investigate the effects of the linear photon momentum on the momentum distributions of photoions and photoelectrons generated in one-photon ionization in an energy range of $300 \text{ eV} \leq E_\gamma \leq 40 \text{ keV}$. Our results show that for each ionization event the photon momentum is imparted onto the photoion, which is essentially the system's center of mass. Nevertheless, the mean value of the ion momentum distribution along the light propagation direction is backward-directed by $-3/5$ times the photon momentum. These results experimentally confirm a 90-year-old prediction.

The electric field vector of an electromagnetic wave is oriented perpendicular to the light propagation axis. As this field drives photoionization, one might expect its direction to be the symmetry axis for angular distributions of photoelectrons and photoions. At high photon energies E_γ and corresponding high photon momenta k_γ, however, this symmetry is violated and the momentum distributions of reaction fragments are asymmetric with respect to the light propagation direction. The observed forward/backward asymmetry of the emitted electrons has puzzled research for the last century (see Refs. [1,2] for reviews). In earliest photoionization studies, performed in 1927, Auger and Perrin left unanswered why their observed forward shift of photoelectrons was "more than 50% higher than the momentum of the photon k_γ" [3]. Later, with the application of wave mechanics on photoionization, calculations reproduced the effect qualitatively and showed that it results from an interference between electric dipole and electric quadrupole transitions (e.g., Ref. [4]), which both alone are forward/backward symmetric. Already Sommerfeld and Schur realized [4] that a mean forward momentum of electrons greater than the photon momentum ($\langle k_x^e \rangle > k_\gamma$) entails that the mean photoion momentum must be backward shifted to account for momentum conservation. The effect has been noticed in the context of radiation pressure in astrophysics [5,6] but received no further attention until recently, when explicit energy-dependent scaling rules were presented in 2014 [7]. Experimentally, the counterintuitive prediction of backward-directed ions created by interaction with light that exerts a forward-directed radiation pressure stands untested until today. In the present work we supply that missing evidence and demonstrate that the backward

momentum of the ion scales with $-(3/5)k_\gamma$ for a wide energy range of 300 eV–40 keV ($k_\gamma = 0.1$–12 a.u.).

In a broader context, the so-called nondipole effects, which result from nonzero photon momentum, also have a significant impact on one-photon multiple ionization [8–12]. There, higher multipole components of the light-matter interaction do not only change the angular distribution of photoelectrons, but also open additional ionization pathways which are dipole forbidden [13]. Recently, nondipole effects have also been studied for absorption of more than one photon [14] up to the extreme regime of strong-field tunnel ionization [7,15–17]. In the strong-field regime, the mechanism responsible for the radiation pressure changes. Here, the action of the magnetic component of the field drives the electron forward, whereas the retardation of the electric field causes the symmetry breaking in the one-photon perturbative regime.

The experiments on one-photon ionization reported here have been performed at beam line P04 at PETRA III (DESY, Hamburg, Germany [18]) using circularly polarized light (low-energy experiment, $E_\gamma = 300$–1775 eV) and beam line ID31 of the European Synchrotron Radiation Facility (ESRF, Grenoble, France) using linearly polarized light (high-energy experiment, $E_\gamma = 12$–40 keV). We have used the ion arm of a COLTRIMS (Cold Target Recoil Ion Momentum Spectroscopy) reaction microscope [19–21] to measure the charge state and the three-dimensional momentum vector of the photoions. The photon beam was crossed at a right angle with a supersonic gas jet of He (low-energy experiment) or N₂ (high-energy experiment). The ions were guided by an electric field to a time- and position-sensitive detector with delay-line position readout [22,23]. From the

ions' times of flight and positions of impact the initial momenta after photoionization were retrieved. For the case of N_2 we considered only K-shell ionization followed by Auger decay. In this case, two singly charged ions are created which we detected in coincidence with the Auger electron. From these three momentum vectors we calculated the momentum of the N_2^+ ion at the instance after photoelectron emission. These results on N_2 are gained from the same experimental runs as Refs. [24,25], where further experimental details can be found. Our spectrometer captured ions with 4π collection solid angle, which allowed us to directly obtain the mean value of the momentum from the data. To access the ion momenta on an absolute scale, it is essential to know precisely the location of ions with zero momentum on our detector. For the high-energy data, this zero point is obtained from ions that are created by Compton scattering. In this case, the photon momentum is transferred to the electron and the ion is thus left with a momentum distribution centered at the origin (see Refs. [26,27] for more detailed discussions of the momentum balance for Compton scattering). For the low-energy data we extrapolate the zero as we show in more detail in Fig. 2.

Figure 1 summarizes the results of our study. Shown in blue is the measured mean value of the ion momentum in direction of the light propagation $\langle k_x^{\text{ion}} \rangle$ as function of photon energy (top scale) or photon momentum (bottom scale). The full circles (low photon energies) correspond to single ionization of He, the full squares (high photon

energies) to K-shell ionization of N_2. In the latter case, as outlined before, the displayed mean value of the sum momentum of both ionic fragments has been adjusted for the momentum of the Auger electron. Negative values correspond to backward emission, i.e., against the photon propagation direction. The corresponding mean value of the photoelectron momentum $\langle k_x^e \rangle$, which is obtained from the measured ion momentum by using momentum conservation ($\langle k_x^e \rangle = -\langle k_x^{\text{ion}} \rangle + k_\gamma$), is plotted in red. The red and blue lines show the corresponding prediction from [7]

$$\langle k_x^{\text{ion}} \rangle = -\frac{3}{5}\frac{E_\gamma - I_P}{c} + \frac{I_P}{c} = -\frac{3}{5}k_\gamma \bigg|_{I_P=0} \quad (1)$$

and

$$\langle k_x^e \rangle = \frac{8}{5}\frac{E_\gamma - I_P}{c} = \frac{8}{5}k_\gamma \bigg|_{I_P=0}, \quad (2)$$

where I_P is the ionization potential and c is the speed of light. Our finding thus yields direct experimental confirmation of the long-standing prediction of backward-directed ion emission in photoionization [4–7].

A fully differential view of the momentum distributions, which underlie the mean value, clearly visualizes the physics origin of the observed ion backward emission.
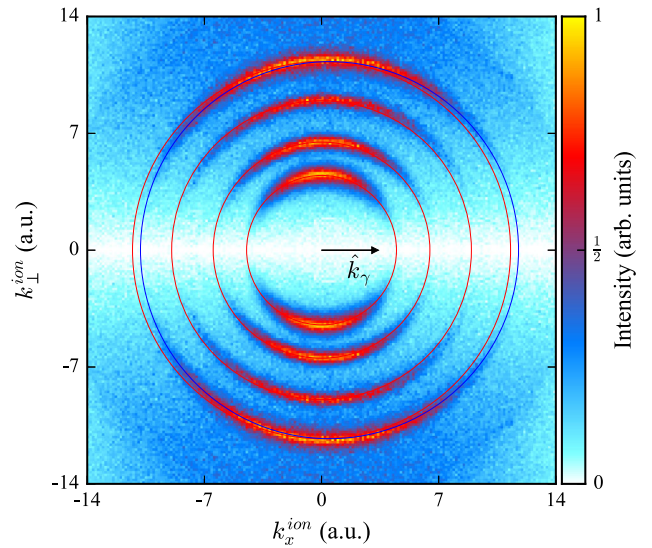
FIG. 2. Momentum distribution of He$^+$ ions from single ionization by circularly polarized photons with $E_\gamma = 300$, 600, 1125, and 1775 eV (from inner to outer ring). Horizontal axis: momentum component parallel to light propagation axis. Vertical axis: momentum perpendicular to the light propagation. The lower half is a mirror image of the upper half of the figure. The red circles are centered at the origin with a radius of the electron momentum $k^e = \sqrt{2(E_\gamma - I_P)}$. The blue outer circle is forward shifted by the corresponding photon momentum $k_\gamma = 0.476$ a.u.. The data from the different photon energies are arbitrarily normalized to match the color scale.
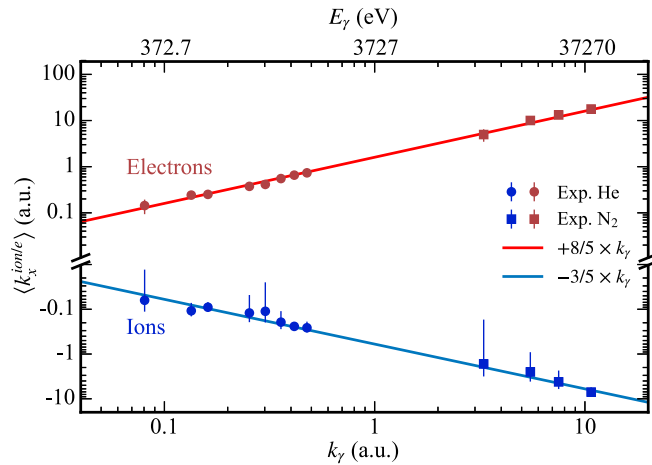

FIG. 1. Mean value of electron (red) and ion (blue) momenta along the light propagation axis after one-photon ionization. Horizontal axis: Photon momentum $k_\gamma = E_\gamma/c$ (bottom scale) and photon energy (top scale). Circles: He photoionization (circularly polarized light); squares: N_2 K-shell photoionization followed by Auger decay, where the mean value corresponds to the sum of both N^+ fragments adjusted for the Auger electron (linearly polarized light). The lines show Eqs. (1) and (2), respectively. Note that in order to compare the He and the N_2 data sets, I_P was approximated as zero in this figure. The error bars are asymmetric only because the y axis is logarithmic.

Figure 2 shows the measured photoion momentum distributions for photoionization of He by 300, 600, 1125, and 1775 eV circularly polarized photons in cylindrical coordinates. The horizontal axis is the momentum component parallel to k_γ, the vertical axis is the momentum perpendicular to the photon axis. By definition this momentum is positive, we have mirrored the distribution at the horizontal axis. The datasets from the different photon energies are normalized to result in the same maximum intensity for better visibility. The red circles represent concentric rings centered on the origin in momentum space. Their radii correspond to the respective photoelectron momenta $k^e = \sqrt{2(E_\gamma - I_P)}$. The events do not accumulate on these rings, but are shifted forward in direction of photon propagation. This is most clearly visible at the outermost ring corresponding to 1775 eV photon energy. The shift of the experimental distributions is given by the respective photon momentum. To guide the eye, the blue circle is shifted forward by the photon momentum of a 1775 eV photon (0.476 a.u.). Hence, the measured ion momentum distributions directly show that the photon momentum is mostly absorbed by the ion, which is strictly a consequence of momentum conservation. In each individual ionization event, the photon momentum is transferred to the center of mass of the system, which almost coincides the ion. Accordingly, the corresponding momentum distribution of the electron shows a circle of the same radius, but not forward shifted. A full derivation of the kinematics including higher order corrections can be found in Ref. [19].

Besides the forward shift of the ring in the ion momentum space, also the distribution of counts on that ring changes with photon energy. This distribution is tilted more to the backward hemisphere upon increase of E_γ. Momentum conservation demands that the measured ion's final momentum equals the photon momentum (causing the forward shift of the sphere) minus the photoelectron momentum. Thus, the distribution of the ions on the shifted sphere in momentum space and the angular distribution of the photoelectrons in the laboratory frame are direct mirror images of each other. These electron angular distributions obtained from our measured ion momentum distributions are shown in Fig. 3. They have an approximate dipolar shape as the initial state is He(1s) and thus the leading angular momentum term in the final state is a dipole ($l = 1$). In addition, this dipolar shape is forward tilted. In order to characterize this effect by an appropriate differential cross section, the dipole approximation has to be extended by a leading first-order correction, i.e., the interference term between the electric dipole (E1) and quadrupole transitions (E2). Accordingly, the angle-differential cross section for photoionization can be written as

$$\frac{d\sigma}{d\vartheta} \propto 1 - \beta\frac{3\cos^2\vartheta - 1}{4} + \gamma\frac{\sin^2\vartheta\cos\vartheta}{2} \qquad (3)$$
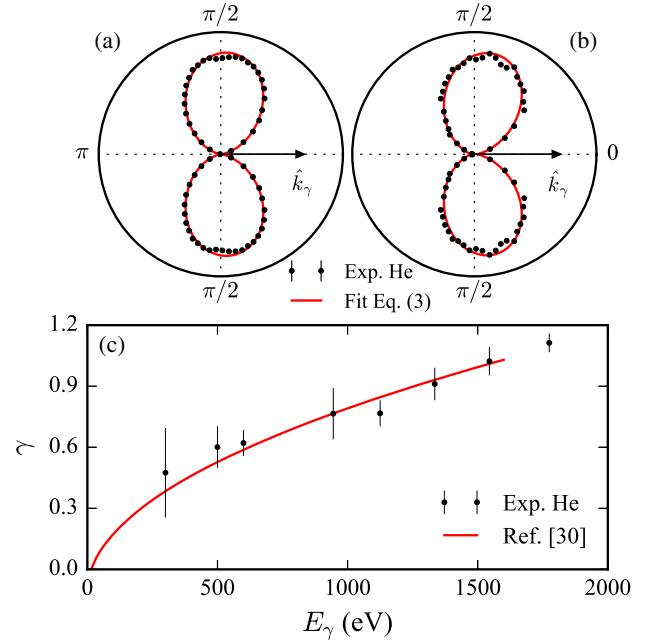

FIG. 3. Electron angular distributions after single ionization of He obtained from the measured ion momentum distributions shown in Fig. 2, using $k^e = -k^{ion} + k_\gamma$. (a) $E_\gamma = 300$ eV, (b) $E_\gamma = 1775$ eV. Red line: Fit using Eq. (3). (c) Nondipole parameter γ from fit of Eq. (3) to the data. Red line: Calculations from Ref. [30].

for circularly polarized (and unpolarized) light [28,29]. Here, β is the dipole anisotropy parameter, γ is the nondipole parameter characterizing the E1-E2 interference, and ϑ is the angle enclosed by photon and photoelectron momenta. Angle-differential cross sections are shaped by the coherent superposition of all possible angular momentum channels of the photoelectron. For a He atom, the dependence of γ on the energy is well reproduced by theory: Our data are in good agreement with published data from Ref. [30]. Note that in the case of N_2 K-shell photoionization at the high photon energies ($E_\gamma = 12$–40 keV), Eq. (3) must be extended by even higher-order corrections to properly describe the angle-differential cross section of photoelectrons [24].

There are many misleading formulations on the photon momentum transfer in the literature. Often, it is sloppily stated that the "absorbed photon imparts its own momentum to the ejected electron" [31] suggesting that this "kick" is responsible for the forward tilt of electron angular distributions as shown in Fig. 3. For a more accurate formulation, it is instructive to recapitulate how the photon momentum transfer emerges from the interaction with the electromagnetic field. For simplicity, we consider photoionization of the 1s electron of the hydrogen atom and follow the formalism of [32]. Beyond the electric dipole approximation, an ionizing plane electromagnetic wave with the wave vector $|k_\gamma| = k_\gamma = E_\gamma/c$ (photon momentum) imprints the local phase factor $e^{ik_\gamma \cdot r}$ in the total

transition matrix element. By introducing the coordinate $\boldsymbol{R}_H$ for the center of mass of the atom and the coordinate $\boldsymbol{r}'$ for the 1s electron with respect to $\boldsymbol{R}_H$, the absolute coordinate of the 1s electron in the laboratory frame can be rewritten as $\boldsymbol{r} = \boldsymbol{R}_H + \boldsymbol{r}'$. The respective phase can thus be factorized as follows:

$$e^{i\boldsymbol{k}_\gamma \cdot \boldsymbol{r}} = e^{i\boldsymbol{k}_\gamma \cdot \boldsymbol{R}_H} e^{i\boldsymbol{k}_\gamma \cdot \boldsymbol{r}'}. \qquad (4)$$

This phase, introduced by the field, modifies the full transition matrix element: The first factor from Eq. (4) enters the transition matrix element $\langle \boldsymbol{\pi}|e^{i\boldsymbol{k}_\gamma \cdot \boldsymbol{R}_H}|\boldsymbol{\pi}_0\rangle$ between the translational states of the atomic center of mass, which are described by the plane waves $(2\pi)^{-3/2} e^{i\boldsymbol{\pi}\cdot\boldsymbol{R}_H}$ with momentum $\boldsymbol{\pi}$. This amplitude yields the momentum conservation law $\boldsymbol{\pi} = \boldsymbol{\pi}_0 + \boldsymbol{k}_\gamma$. Thus, a photon absorption by the atom introduces to its center of mass the momentum $\boldsymbol{k}_\gamma$. The second phase factor $e^{i\boldsymbol{k}_\gamma \cdot \boldsymbol{r}'}$ from Eq. (4) enters the electric dipole transition matrix element and is responsible for the multipole (retardation) corrections beyond the electric dipole approximation.

The photon momentum and nondipolar photoionization are of relevance in many areas such as astrophysics of stellar outer layers [33] or for acceleration of electrons by relativistic laser pulses [34]. The simplest and most transparent process where the photon momentum manifests is one-photon excitation where the atom receives the photon momentum, providing, for example, a tool for laser cooling. Above the ionization threshold in each ionization event, the ion receives the photon momentum and in addition the recoil of the photoelectron. The additional orbital angular momentum transfer from the photon leads to an increasing forward tilt of the electron angular distribution. This forward-directed mean momentum of the electron is balanced by a backward-directed momentum transfer to the ion. Our results show that for s-initial states, the ion backward momentum scales with $-(3/5)k_\gamma$, confirming a long-standing prediction. For more complex processes like double ionization [12], the photon momentum sharing is less straightforward in detail, the ion backward emission, however, prevails. This is very different for multiphoton processes in strong laser pulses where electrons are forward driven by the magnetic component of the light field [7,14–16]. Our present observation on ion momenta can be extended in the future to ionization in the multiphoton regime in order to test the prediction that high fields direct the ions forward [7].

[*]grundmann@atom.uni-frankfurt.de
[†]kircher@atom.uni-frankfurt.de
[‡]doerner@atom.uni-frankfurt.de

[1] J. G. Jenkin, J. Electron Spectrosc. Relat. Phenom. **23**, 187 (1981).
[2] O. Hemmers, R. Guillemin, and D. W. Lindle, Radiat. Phys. Chem. **70**, 123 (2004).
[3] P. Auger and F. Perrin, J. Phys. Radium **8**, 93 (1927).
[4] A. Sommerfeld and G. Schur, Ann. Phys. (N.Y.) **396**, 409 (1930).
[5] G. Michaud, Astrophys. J. **160**, 641 (1970).
[6] M. J. Seaton, J. Phys. B **28**, 3185 (1995).
[7] S. Chelkowski, A. D. Bandrauk, and P. B. Corkum, Phys. Rev. Lett. **113**, 263005 (2014).
[8] J. S. Briggs and V. Schmidt, J. Phys. B **33**, R1 (2000).
[9] M. Y. Amusia, E. G. Drukarev, V. G. Gorshkov, and M. P. Kazachkov, J. Phys. B **8**, 1248 (1975).
[10] M. S. Schöffler, C. Stuck, M. Waitz, F. Trinter, T. Jahnke, U. Lenz, M. Jones, A. Belkacem, A. L. Landers, M. S. Pindzola, C. L. Cocke, J. Colgan, A. Kheifets, I. Bray, H. Schmidt-Böcking, R. Dörner, and T. Weber, Phys. Rev. Lett. **111**, 013003 (2013).
[11] S. Grundmann, F. Trinter, A. W. Bray, S. Eckart, J. Rist, G. Kastirke, D. Metz, S. Klumpp, J. Viefhaus, L. P. H. Schmidt, J. B. Williams, R. Dörner, T. Jahnke, M. S. Schöffler, and A. S. Kheifets, Phys. Rev. Lett. **121**, 173003 (2018).
[12] S.-G. Chen, W.-C. Jiang, S. Grundmann, F. Trinter, M. S. Schöffler, T. Jahnke, R. Dörner, H. Liang, M.-X. Wang, L.-Y. Peng, and Q. Gong, Phys. Rev. Lett. **124**, 043201 (2020).
[13] F. Maulbetsch and J. S. Briggs, J. Phys. B **28**, 551 (1995).
[14] S. Chelkowski, A. D. Bandrauk, and P. B. Corkum, Phys. Rev. A **95**, 053402 (2017).
[15] C. T. L. Smeenk, L. Arissian, B. Zhou, A. Mysyrowicz, D. M. Villeneuve, A. Staudte, and P. B. Corkum, Phys. Rev. Lett. **106**, 193002 (2011).
[16] A. Ludwig, J. Maurer, B. W. Mayer, C. R. Phillips, L. Gallmann, and U. Keller, Phys. Rev. Lett. **113**, 243001 (2014).
[17] A. Hartung, S. Eckart, S. Brennecke, J. Rist, D. Trabert, K. Fehre, M. Richter, H. Sann, S. Zeller, K. Henrichs, G. Kastirke, J. Hoehl, A. Kalinin, M. S. Schöffler, T. Jahnke, L. P. H. Schmidt, M. Lein, M. Kunitski, and R. Dörner, Nat. Phys. **15**, 1222 (2019).
[18] J. Viefhaus, F. Scholz, S. Deinert, L. Glaser, M. Ilchen, J. Seltmann, P. Walter, and F. Siewert, Nucl. Instrum. Methods Phys. Res., Sect. A **710**, 151 (2013).
[19] R. Dörner, V. Mergel, O. Jagutzki, L. Spielberger, J. Ullrich, R. Moshammer, and H. Schmidt-Böcking, Phys. Rep. **330**, 95 (2000).
[20] J. Ullrich, R. Moshammer, A. Dorn, R. Dörner, L. P. H. Schmidt, and H. Schmidt-Böcking, Rep. Prog. Phys. **66**, 1463 (2003).

[21] T. Jahnke, T. Weber, T. Osipov, A. L. Landers, O. Jagutzki, L. P. H. Schmidt, C. L. Cocke, M. H. Prior, H. Schmidt-Böcking, and R. Dörner, J. Electron Spectrosc. Relat. Phenom. **141,** 229 (2004).

[22] O. Jagutzki, J. S. Lapington, L. B. C. Worth, U. Spillman, V. Mergel, and H. Schmidt-Böcking, Nucl. Instrum. Methods Phys. Res., Sect. A **477,** 256 (2002).

[23] O. Jagutzki, V. Mergel, K. Ullmann-Pfleger, L. Spielberger, U. Spillmann, R. Dörner, and H. Schmidt-Böcking, Nucl. Instrum. Methods Phys. Res., Sect. A **477,** 244 (2002).

[24] M. Kircher, J. Rist, F. Trinter, S. Grundmann, M. Waitz, N. Melzer, I. Vela-Pérez, T. Mletzko, A. Pier, N. Strenger, J. Siebert, R. Janssen, L. P. H. Schmidt, A. N. Artemyev, M. S. Schöffler, T. Jahnke, R. Dörner, and P. V. Demekhin, Phys. Rev. Lett. **123,** 243201 (2019).

[25] M. Kircher, J. Rist, F. Trinter, S. Grundmann, M. Waitz, N. Melzer, I. Vela-Pérez, T. Mletzko, A. Pier, N. Strenger, J. Siebert, R. Janssen, V. Honkimäki, J. Drnec, P. V. Demekhin, L. P. H. Schmidt, M. S. Schöffler, T. Jahnke, and R. Dörner, Phys. Rev. Lett. **123,** 193001 (2019).

[26] L. Spielberger, O. Jagutzki, R. Dörner, J. Ullrich, U. Meyer, V. Mergel, M. Unverzagt, M. Damrau, T. Vogt, I. Ali, K. Khayyat, D. Bahr, H. G. Schmidt, R. Frahm, and H. Schmidt-Böcking, Phys. Rev. Lett. **74,** 4615 (1995).

[27] M. Kircher, F. Trinter, S. Grundmann, I. Vela-Perez, S. Brennecke, N. Eicke, J. Rist, S. Eckart, S. Houamer, O. Chuluunbaatar, Y. V. Popov, I. P. Volobuev, K. Bagschik, M. N. Piancastelli, M. Lein, T. Jahnke, M. S. Schöffler, and R. Dörner, Nat. Phys., (2020).

[28] J. W. Cooper, Phys. Rev. A **42,** 6942(R) (1990).

[29] J. W. Cooper, Phys. Rev. A **47,** 1841 (1993).

[30] M. Y. Amusia, A. S. Baltenkov, L. V. Chernysheva, Z. Felfli, and A. Z. Msezane, Phys. Rev. A **63,** 052506 (2001).

[31] H. A. Bethe and E. E. Salpeter, *Quantum Mechanis of One- and Two-Electron Atoms* (Springer, Berlin, 1957).

[32] V. C. Felicissimo, F. F. Guimaraes, and F. Gel'mukhanov, Phys. Rev. A **72,** 023414 (2005).

[33] M. J. Seaton, Astrophys. Space Sci. **237,** 107 (1996).

[34] A. Di Piazza, C. Müller, K. Z. Hatsagortsyan, and C. H. Keitel, Rev. Mod. Phys. **84,** 1177 (2012).